Journal of Polymers and the Environment (2021) 29:3288–3301
https://doi.org/10.1007/s10924-021-02118-1

ORIGINAL PAPER

Blends of Poly (Butylene Adipate-Co-Terephthalate) and Thermoplastic Whey Protein Isolate: A Compatibilization Study

Marina Fernandes Cosate de Andrade[1] · Hugo Campos Loureiro[2] · Claire Isabel Grígoli de Luca Sarantopóulos[3] · Ana Rita Morales[1]

Accepted: 8 March 2021 / Published online: 18 March 2021

Abstract

This work assesses the influence of the plasticizer polyethylene glycol (PEG) on the compatibilization of poly (butylene adipate-co-terephthalate) (PBAT) and thermoplastic whey protein isolate (WPIT) blends. To prepare the blends, WPI was denatured at 90 °C, in the presence of PEG, to become a thermoplastic material. Dried WPIT was later mechanically blended with PBAT using a torque rheometer at 160 °C and 80 rpm. Two blends were prepared: 90% of PBAT/10% of WPIT (90_10) and 70% of PBAT/30% of WPIT (70_30). Scanning electron microscopy (SEM) analyses showed a homogenous blend morphology and good interaction between the dispersed phase and the matrix. Atomic force microscopy-based infrared spectroscopy (AFM-IR) showed PBAT and WPIT bands in all studied regions of both blends, which suggests that these materials presented partial miscibility. The viscosity ratio of the PBAT/WPIT system was less than 3.5 in the high shear rate region in complex viscosity curves, which indicates that droplet break-up of WPIT may occur by the drop fibrillation mechanism. The addition of WPIT reduced the degree of crystallinity of PBAT in the blends in comparison to pristine PBAT as shown by X-ray diffraction (XRD). Mechanical tests showed that blend tensile strength and elongation at break decreased with the addition of WPIT. Elastic modulus of the blends increased compared to pristine PBAT. Barrier properties were also evaluated showing that the oxygen permeability coefficient reduced by 20% for the blend with 30% of WPIT and vapor water permeability increased with the addition of WPIT.

Keywords PBAT · Biopolymer · Compatibilization · PEG · Polymer blends

Introduction

The study of materials from renewable resources is an important issue nowadays. The use of petroleum releases a fossil carbon that was previously locked up and contributes to climate change due to the greenhouse effect while renewables follow a carbon cycle that is carbon–neutral [1]. Proteins such as soy protein isolate [2], sunflower protein isolate (SFPI) [3], whey protein isolate [4], among others, could be investigated as options to replace fossil materials. Whey protein isolate (WPI) is a biobased and biodegradable polymer with great oxygen barrier properties and its modification has been studied to be used in packaging industries [4, 5]. WPI is used as a raw material for Wheylayer®, a compound utilized in multilayer packaging, which presents good oxygen and water vapor barrier properties, comparable to poly(ethylene-co-vinyl alcohol) (EVOH) [4].

One important aspect related to WPI is its high glass transition temperature (Tg), fragility and difficult processing. To improve WPI mechanical properties and decrease its Tg, native protein is submitted to denaturation, a heat treatment that develops protein structure unfolding and allows the formation of intermolecular interactions [6, 7], in the presence of water and plasticizers such as glycerol [8–11], which generates a thermoplastic whey protein isolate (WPIT).

Some renewable materials still present limitations to their use in packaging applications, such as poor mechanical properties and thermal stability. To improve these features,

✉ Ana Rita Morales
morales@unicamp.br

[1] DEMBio, School of Chemical Engineering, University of Campinas (UNICAMP), Avenida Albert Einstein, 500, Campinas, SP CEP 13083-852, Brazil

[2] Institute of Chemistry, University of Campinas (UNICAMP), Campinas, SP, Brazil

[3] Institute of Food Technology, Av. Brasil, 2880, Campinas, SP 13070-178, Brazil

one potential solution is to blend renewable polymers with commercial polymers [12]. WPIT was studied in blends with polymers such as starch [13], poly (butylene succinate) (PBS) [14] or ethylene vinyl acetate (EVA) [15]. This last blend showed improved oxygen barrier in relation to pure EVA.

Poly (butylene adipate-co-terephthalate) (PBAT), a biodegradable aliphatic–aromatic copolymer, presents mechanical properties comparable to low density polyethylene [16–18], and is used mainly as film for agriculture and food packaging [19, 20]. PBAT was used as a component in blends with biobased polymers, such as soy protein concentrate [21, 22] and soy protein isolate [23]. Nevertheless, those blends of proteins and commercial polymers may be immiscible, incompatible, and not present the expected properties [12].

Blend compatibilization is used to improve the properties of immiscible and partially miscible blends, since most polymer blends are not thermodynamically miscible [12]. The compatibilizer reduces interfacial tension and enables dispersion, stabilizes morphology against destructive modifications during processing, and improves adhesion between phases in the solid state, which contributes to stress transfer [24] and prevents the occurrence of cracks initiated at the growth interface until the appearance of a catastrophic failure [25]. In addition, the compatibilizer can transform the coarse morphology of the immiscible blends into a reduced size morphology that may improve their desired properties [12].

In systems of protein and commercial polymer blends studied, an external compatibilizer proved to enhance their compatibility, such as chain extenders and 2-methylimidazole (2MI) for PBAT/Novatein thermoplastic protein [26] and maleic anhydride grafted PBAT for PBAT/soy protein concentrate (SPC) blends [21]. Besides compatibility, plastification plays an important role in these blends. Glycerol is one of plasticizers most commonly used in proteins [27] but some lack of miscibility has been reported [14].

Blends of PBAT/WPIT, in which glycerol was used as plasticizer, were studied in a previous work [28]. The blends, processed by melting, resulted in immiscible and non-compatibilized morphology that was explained by the elastic rheological behavior of PBAT and WPIT at processing conditions. These previous results motivated us to consider an alternative to improve the protein/polymer system compatibility by using a plasticizer compatible with both polymers, PBAT and WPIT. Polyethylene glycol (PEG) is considered miscible when blended with PBAT and presents high affinity with hydrophilic compounds [29]. Thus, PEG could be a good option to be studied in a PBAT/WPIT system due to its affinity with both hydrophobic materials such as PBAT and hydrophilic materials such as WPI.

The goal of this work was to assess the influence of PEG as plasticizer of WPIT on the compatibilization of PBAT/WPIT blends by studying their mechanical, morphological, thermal, barrier and rheological properties.

Materials and Methods

Materials

The following materials were used in this work: PBAT Ecoflex F Blend C1200 (BASF), Hilmar™ 9010 Instantized Whey Protein Isolate (WPI) (Hilmar Ingredients), polyethylene glycol (PEG) 400 for synthesis (Merck), and sodium sulfite (Synth).

Methods

To predict the miscibility level between polymers and plasticizers, solubility parameters and the Flory Huggins's interaction parameter of the pairs were calculated using the methodology described in Krevelen et al. [30].

Blends were prepared following three steps:

Step 1. WPIT Preparation

For the WPIT preparation, 34.9% of WPI (wt%), 35.1% of PEG (wt%), 30.0% of deionized water (wt%), and 2% of sodium sulfite (wt% in relation to WPIT content) were mixed using a mechanical stirrer with a dissolver stirrer at 470 rpm for 30 min. This mixture was heated at 90 °C for 30 min in an oven followed by cooling at room temperature. It was cut into small pieces and dried in a vacuum oven at 40 °C for 90 h. Dried WPIT was milled in a Freezer/Mill 6870 cryogenic mill from SPEX Sample Prep at the following conditions: 5 cycles of 5 min of pre-cooling in liquid nitrogen, running time of 2 min, cooling time in liquid nitrogen of 1 min, and rate of 10 cps. After milling, WPIT sieving was performed according to ASTM D1921-18, method B [32]. Four sieving batches were carried out with two sieves of Tyler 20 and Tyler 25 for 20 min. Lyophilization of milled WPIT was performed by direct freezing in liquid nitrogen and frozen samples were placed in the LabConco lyophilizer and left there for 24 h.

Step 2. Preparation of PBAT/WPIT Blends

PBAT was dried at 70 °C for 1 h before processing. The blends, whose compositions are shown in Table 1, were processed using a HAAKE PolyLab OS RheoDrive seven equipped with a HAAKE Rheomix 3000OS torque rheometer using roller rotors with net chamber volume of 310 cm^3, at 160 °C and 80 rpm for 6 min.

Table 1 Composition of PBAT/WPIT blends

Sample	PBAT		WPIT		Processing time (min)
	(%)	(g)	(%)	(g)	
PBAT	100	230	–	–	6
90_10	90	207	10	23	6
70_30	70	161	30	69	6

Step 3. Film Manufacturing

Films were prepared by hot pressing in a hydraulic press from MH Equipamentos, model MH-P8HR PN in a square mold made of Teflon, at 8 ton for 5 min at 130 °C for blends and at 150 °C for PBAT. The films were cooled during pressing to room temperature at 8 ton for 1 min and 30 s.

Characterization

Torque vs. time curves were obtained during processing by torque rheometer.

A rheometer with parallel-plate geometry from TA Instruments DHR 2 was used to obtain rheological properties of PBAT, WPIT and blends. The gaps of the plates presented a distance of 1 mm. The linear viscoelastic region of both polymers was measured by strain sweep test. The angular frequency range of 0.01 to 500 rad/s at 160 °C was used to obtain the dynamic frequency sweep measurements. Pellets of PBAT and pieces of blends were pressed in the shape of a disk at 160 °C for 3 min using a hydraulic press from MH Equipamentos, model MH-P8HR PN. WPIT was tested as powder. Storage modulus (G´), loss modulus (G´´), complex viscosity (η*) and complex viscosity ratio (p) were obtained.

Scanning electron microscopy (SEM) was used to analyze film fracture morphologies which were cryofractured by cooling in liquid nitrogen. Samples were covered by a ~ 16 nm gold layer by sputtering. A FEI Inspect F50 scanning electron microscope was used to obtain images operating at 10 kV.

As first observed by SEM, the blends presented two-phase morphology and atomic force microscopy-based infrared spectroscopy (AFM-IR) was used as a powerful technique to detect the presence of each material in each phase of the PBAT/WPIT blends. This technique consists in focusing the IR laser in the direction of the sample at the location of the AFM probe tip (cantilever). When the wavelength coincides with material absorption bands, a rapid thermal expansion occurs, which causes oscillations in the cantilever that are measured by AFM. Spectrum is obtained by measuring the oscillation amplitude of the cantilever as a function of IR wavelength [33]. Carbonyl stretching bands were monitored to identify PBAT and amide I bands for WPIT. The blends were cut in sections of 80 nm with a DDK tungsten carbide knife at − 110 °C using a Leica Reichert Ultracut FC6ultramicrotome. Samples were deposited in silicon plates previously covered with gold. The equipment used was a ANASYS NanoIR2-s atomic force microscope (BRUKER) in contact mode and a BudgetSensors ContGB-G tip. The analyses were performed in the region 1560–1820 cm^{-1} with a resolution of 2 cm^{-1}. Spectra of PBAT and WPIT were also obtained for reference.

X ray diffraction (XRD) was used in order to acquire the degree of crystallinity of PBAT in the blends using a Philips Analytical X Ray, X´Pert-MPD diffractometer supplied with a filter radiation of Cu-Kα (λ = 1.54056 Å) under the following conditions: voltage of 40 kV, range of 5 to 40° (2θ), speed of 0.02°/s, current of 40 mA and step of 0.02°. The degree of crystallinity was obtained by the ratio of the sum of crystalline peak areas to the sum of crystalline peaks and amorphous halo areas. The areas of peaks and halos were acquired by XRD deconvolution, which was performed using OriginPro 8.1 and shaping the peaks and halos according to the Gaussian function.

Thermal stability of the materials was obtained by Thermogravimetric analyses (TGA) in accordance with ASTM E2550-11 [34] using a TGA 2950 analyzer from TA Instruments. Samples were heated from room temperature to 600 °C at a rate of 10 °C/min at inert atmosphere. For each blend, an additivity curve of thermogravimetric results was calculated, which consists of the mass contribution of the thermogravimetric curve of each blend component. It represents a trend that is expected if there is no interaction between the blend components.

Differential scanning calorimetry (DSC) was performed to evaluate thermal transitions of the materials using a DSC Q100 from TA Instruments. Samples were cooled from room temperature to − 80 °C at a cooling rate of 10 °C/min, kept at − 80 °C for 5 min and heated from − 80 °C to 200 °C at a heating rate of 10 °C/min, and kept at 200 °C for 5 min. All analyses were performed under inert atmosphere.

Tensile tests were conducted using an EMIC universal test machine model DL 2000 in accordance with ASTM D882-12 [35]. Films were cut into the following dimensions: 100 mm × 25 mm × 320 µm (average thickness). The load cell was 5000 N, the test speed was 500 mm/min and the distance between grips was 50 mm. Elastic modulus, tensile strength at break and elongation at break were obtained. Student's t-test with a significance level of 0.05 validated statistically the results.

The oxygen transmission rates (OTR) of PBAT and blends were measured by coulometric method, according to ASTM F1927 [36] using OX-TRAN, model 2/22 MOCON, with pure oxygen as a permeant gas. Specimen conditioning and tests were carried out at 23 °C, 50% RH for 48 h. The test area of each specimen was 5 cm^2. Tests were performed in duplicate for each sample. OTR values were used

to calculate the oxygen permeability coefficient (P'O_2) (mL (STP) mm.m^{-2}.day^{-1}.atm^{-1}), according to Eq. 1 [36].

$$P'O_2 = \frac{OTR.e}{p} \quad (1)$$

where OTR is the oxygen transmission rate (mL (STP).m^{-2}.day^{-1}), e is the average thickness of specimens (mm) and p is the oxygen partial pressure gradient across the film, which is equal to 1 atm.

The water vapor transmission rates (WVTR) of PBAT and blends were measured using PERMATRAN, an equipment with infrared sensor, model W 3/34 MOCON, according to ASTM F1249 [37]. Tests were conducted at 38 °C and 90% RH. The Permeation area of each specimen was 5 cm^2. Tests were performed in duplicate for each sample. WVTR values were used to calculate the water vapor permeability coefficient (WVP) (g.mm.m^{-2}.day^{-1}.$mmHg^{-1}$) according to Eqs. 2 and 3 [37].

$$WVP = \frac{WVTR.e}{p_{H2O}} \quad (2)$$

$$p_{H2O} = y_{H2O} * P_{sat} \quad (3)$$

where WVTR is the water vapor transmission rate (g.m^{-2}.day^{-1}), e is the average thickness of specimens (mm), P_{H2O} is the partial pressure gradient of water across the sample, y_{H2O} is the molar fraction of water vapor (0.9) and P_{sat} is the water vapor pressure at the test temperature (49.692 mmHg at 38 °C).

Results and Discussion

The first consideration for this study was the prediction of miscibility between the components. Table 2 presents solubility parameters of WPI, PBAT, glycerol and PEG. This analysis shows that the hydrogen bond component of the solubility parameter (δh) of PEG is closer to PBAT and WPI in relation to glycerol, which may indicate some difference in the compatibility of plasticizers with PBAT and WPI.

Table 2 Solubility parameters (δ) of WPI, PBAT, glycerol and PEG

Polymer	δd $(MPa)^{0.5}$	δp $(MPa)^{0.5}$	δh $(MPa)^{0.5}$	δt $(MPa)^{0.5}$
WPI	17.0	5.8	14.9	23.3
PBAT	18.2	5.1	8.8	20.9
Glycerol [31]	17.4	12.1	29.3	36.2
PEG	17.8	11.1	9.1	22.9

δd Contribution of dispersion forces to the solubility parameter

δp Contribution of polar forces to the solubility parameter

δh Contribution of hydrogen bonding to the solubility parameter

δt Total solubility parameter

The Flory Huggins interaction parameters (χ) calculated for the pairs are shown in Table 3. According to Cosate de Andrade et al. [28], χ of the WPI-PBAT pair was calculated as 0.2, which means the blend between those polymers could be miscible. In addition, glycerol was used considering that it is one of the most commonly used plasticizers for proteins [27], but incompatible blends were obtained [28]. Therefore, it is important to compare glycerol with PEG, which is our option of plasticizer in this work. The PBAT-PEG and WPI-PEG pairs were calculated as 0.2 and 0.0, respectively, while for the PBAT-glycerol and WPI-glycerol pairs we can see χ values of 9.5 and 6.7, respectively. As miscibility is expected for χ values lower than 1 [38], PEG was considered a strong candidate for the purpose of our study and the results could explain the lack of miscibility previously observed for glycerol [28].

Figure 1 shows the rheological behavior of PBAT and blends during processing at the rheometer by the torque x time curves (Fig. 1a) and the maximum torque and steady state torque (Fig. 1b.). Blend melting time was lower with the addition of WPIT in relation to pristine PBAT, as can be seen by the time to reach maximum torque in Fig. 1a. This can be explained by the larger surface area presented by cryogenically milled WPIT particles, which accelerates heat transfer in relation to materials with larger particle size and smaller surface area [39], such as PBAT in granules processed alone. The addition of WPIT reduced the maximum and steady state torque of the blends compared to PBAT. There are two effects that could explain this behavior: PEG acts as a lubricant during processing and the particle size of WPIT is smaller than PBAT, which may favor heat transfer during processing.

Figure 2 shows the rheological curves of pure PBAT and WPIT. PBAT presented a typical thermoplastic behavior with predominance of viscous component (G'') in relation to elastic component (G') (Fig. 2a) as well as the presence of a Newtonian plateau of η* in the terminal zone (Fig. 2c). On the other hand, WPIT showed a predominance of elastic component in the terminal zone (Fig. 2b), which may be explained by the formation of a protein network [40]. Moreover, the WPIT rheology curve presented an approximation of elastic and viscous components at high frequencies, which could be a crossover region, probably due to the destruction

Table 3 Flory Huggins interaction parameter (χ) of PBAT-PEG, WPI-PEG, PBAT-glycerol, and WPI-glycerol pairs

Pair A-B	χ_{A-B}
PBAT-glycerol	9.5
WPI-glycerol	6.7
PBAT-PEG	0.2
WPI-PEG	0.0

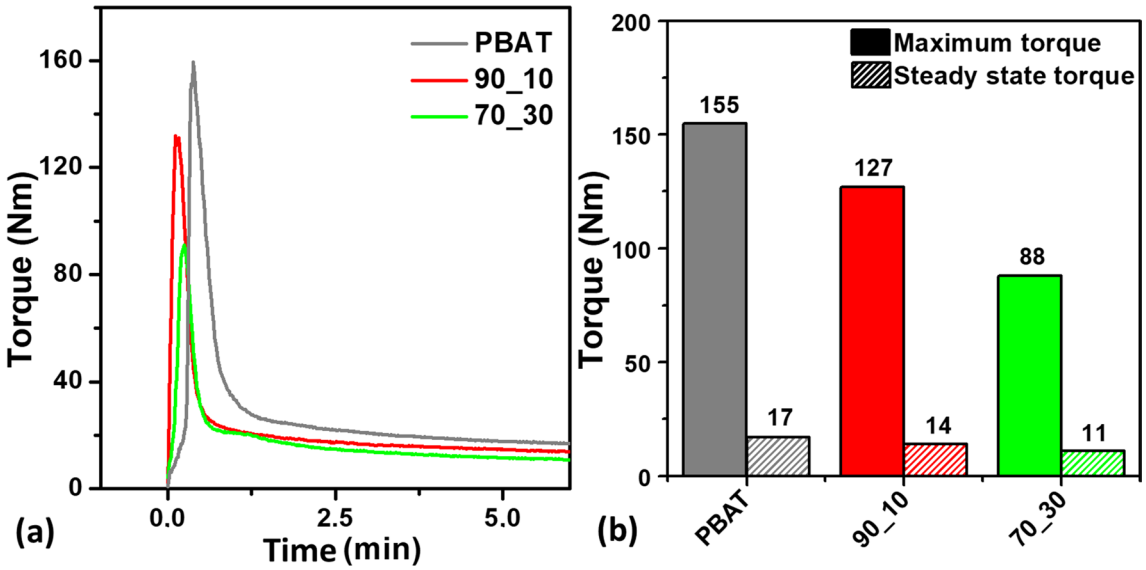

Fig. 1 Behavior of PBAT/WPIT blends on torque rheometer: **a** torque x time curves during processing at 80 rpm and 160 °C and **b** values of maximum and steady state torque of PBAT and PBAT/WPIT blends

of the protein network at high frequencies [22]. The WPIT curve of η* (Fig. 2c) follows the behavior of power law and does not present the Newtonian plateau at the terminal zone, which is a typical behavior of materials with the presence of gel or network [40].

WPIT plasticized with PEG presented a less pronounced elastic component in comparison with WPIT plasticized with glycerol, which was shown in previous work [28]. Probably, there was a reduction in the presence of hydrogen bonds in the protein due to the plasticizer exchange. The hydrogen bond component of the PEG solubility parameter (δh) (δh = 9.1 $MPa^{0.5}$) is lower than the glycerol hydrogen bond solubility parameter (δh = 29.3 $MPa^{0.5}$).

Blend morphology can be influenced by the viscosity ratio (p) (the ratio of WPIT viscosity to PBAT viscosity). According to Lin et al. [41] the droplet break-up may occur by the erosion mechanism for values of $p > 3.5$. A curve of p x angular frequency for the PBAT/WPIT system is shown in Fig. 2d, which shows that an angular frequency of 108 rad/s corresponds to a viscosity ratio of 3.5. There is a region at high frequencies (> 108 rad/s) which presents greater shear and $p < 3.5$. In this region, the viscosities of the dispersed phase and the matrix show closer values, which could favor the occurrence of droplet break-up by the drop fibrillation mechanism. Considering the mixing chamber geometry of the torque rheometer, there are mixing regions with greater shear between the rotor and chamber (favoring drop fibrillation) and other regions with less shear, close to the rotor body (favoring the erosion mechanism). These results suggest that the blends may have undergone different mechanisms during processing.

Figure 3 shows the blend rheometry parameters. Blend behavior seems to be closer to PBAT behavior. This means that PBAT rheological properties prevailed in the blend, although at the high frequency region the blends showed lower values of G´, G´´ and η* compared to pristine components. This is indicative of new interactions between components and the AFM-IR results were helpful to complete the analysis.

SEM micrographs of films fractures of PBAT/WPIT blends are shown in Fig. 4. Fracture surface shows that there was a good homogenization between PBAT and WPIT. In the 90_10 blend the domains were not clearly identified although we observed some regions that look like a second phase in the matrix. No cracks, pores or discontinuous and well-defined interfaces between the phases were observed. This homogeneity in the morphology of the 90_10 blend is a strong indication of certain compatibility between components [42].

Regions with microvoids can be seen in the 70_30 blend, which may be domains of WPIT that were ripped out during the fracture and show lack of adhesion between the dispersed phase and the matrix.

Regarding structural analyses, we performed FTIR (results not shown), but we could not differentiate between bands from the dispersed phase and the matrix due to the small size of the dispersed phase. Atomic force microscopy-based infrared spectroscopy (AFM-IR) was performed and proved to be very sensitive to assess the presence of the specific functional groups of each component in both phases. The presence of stretch bands of PBAT carbonyl and WPIT amide I in blends were considered for AFM-IR analysis. In

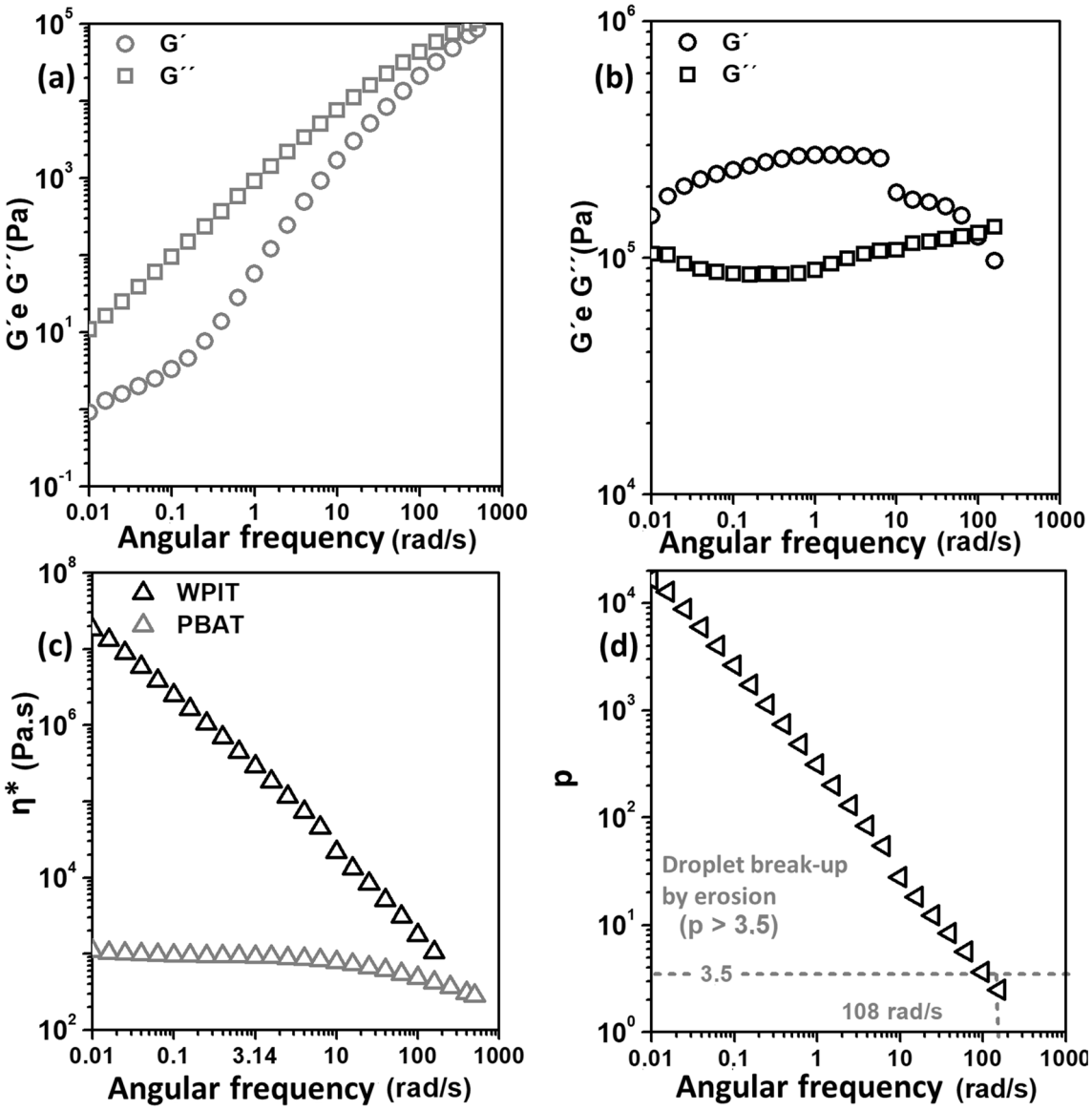

Fig. 2 Rheometry results at 160 °C: storage modulus (G´) and loss modulus (G´´) of: **a** PBAT, **b** WPIT, **c** complex viscosity (η*) of PBAT and WPIT and **d** complex viscosity ratio (p) for the pair

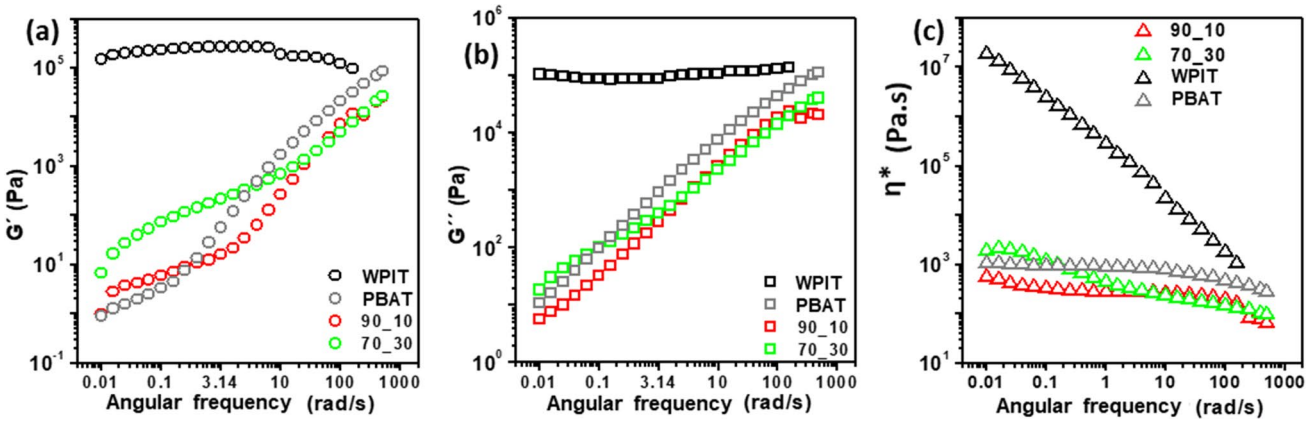

Fig. 3 Rheometry results of PBAT, WPIT and blends: storage modulus (G´) (**a**), loss modulus (G´´) (**b**), and **c** complex viscosity (η*) at 160 °C

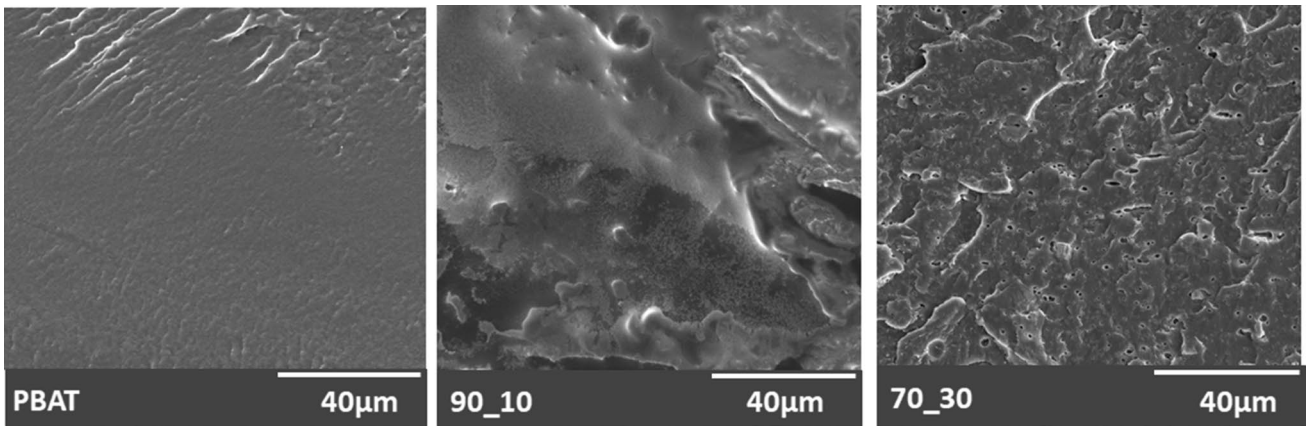

Fig. 4 Images of SEM analyses of PBAT/WPIT blends fractured films

the region from 1570 to 1800 cm^{-1}, which was studied by AFM-IR, PBAT presents a band related to carbonyl stretching [43] in 1728 cm^{-1} and WPIT presents a band associated to amide I band [44] in 1656 cm^{-1}. Figure 5 shows AFM-IR analysis results of the 90_10 blend. Four points were analyzed, two protuberances, i.e., domains of the dispersed phase (1 and 3), and two regions in the plane, i.e., the matrix (2 and 4). Protuberance regions showed WPIT bands in 1628 and 1672 cm^{-1} with greater intensity compared to the PBAT band in 1744 cm^{-1}. Regions in the plane showed PBAT bands with greater intensity compared to WPIT bands.

Figure 6 shows the AFM-IR results for the 70_30 blend. Six regions were analyzed: two protuberances, i.e., domains of the dispersed phase (2 and 5), two depressions, where domains were ripped out (3 and 4), and two regions in the plane, located in the matrix (1 and 6). In the studied regions, six points showed bands related to PBAT in 1738 cm^{-1} and WPIT in 1624 cm^{-1} with similar proportional intensities, which is an evidence of the presence of both polymers in all studied regions.

AFM-IR results represent a strong indication that the PBAT/WPIT/PEG system is partially miscible when processed at studied conditions in a torque rheometer. This would be possible considering the values obtained for the Flory–Huggins interaction parameter (Table 3), which showed that the PBAT-PEG, WPI-PEG and PBAT-WPI systems have chemical affinity. For both blends there was a slight band shift of the PBAT phase in the blend in relation to pristine PBAT. In the WPIT phase of both blends there was a conformation change of pre-processing protein to alpha helix (1656 cm^{-1}) for the formation of beta sheet structures with the presence of very strong hydrogen bonds [45] after blend processing, which would be represented by: two bands in 1628 and 1672 cm^{-1} in 90_10 blend spectra and a band in 1624 cm^{-1} in 70_30 blend spectra. This may be an evidence of formation of new interactions between WPI and PEG after exposure to heat and shear from blend processing.

Figure 7 shows the diffractogram (Fig. 7a) and degree of crystallinity (Fig. 7b) of WPI, WPIT, PBAT and blends.

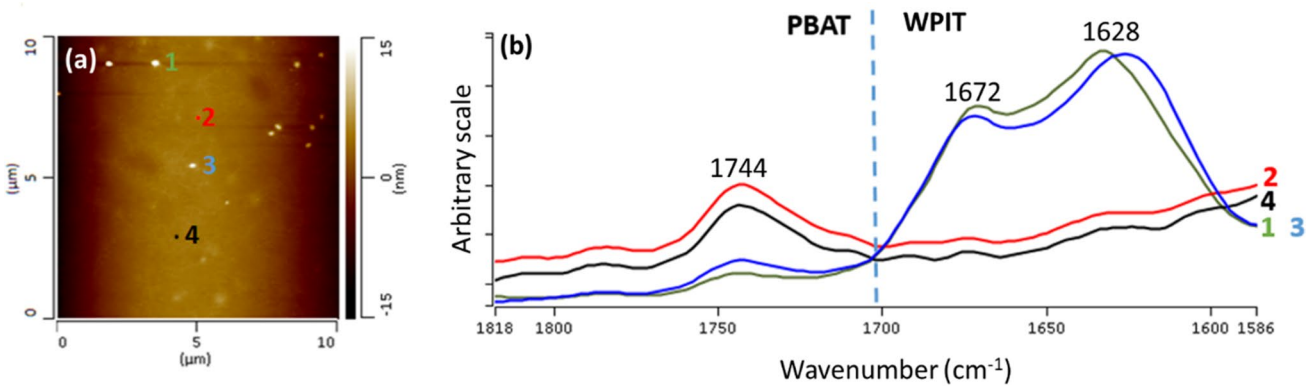

Fig. 5 AFM-IR analysis of 90_10 blend. **a** Topography of analyzed region. **b** IR spectra of four points studied

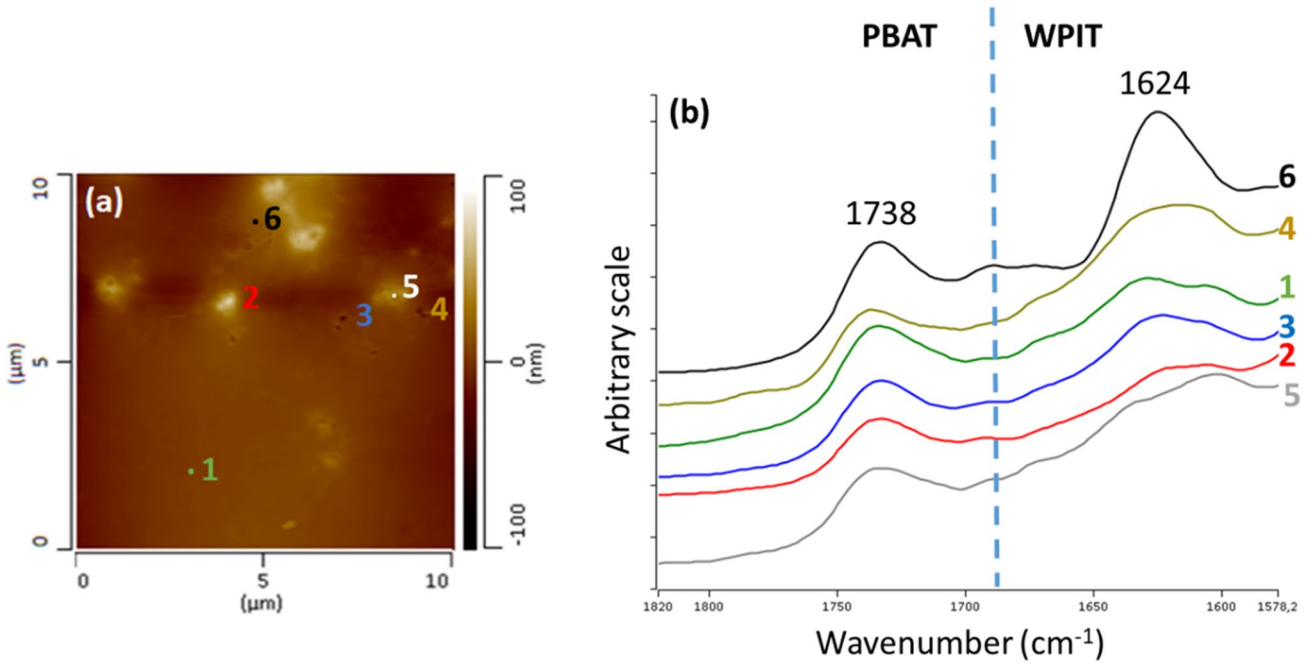

Fig. 6 AFM-IR analysis of 70_30 blend. **a** Topography of analyzed region. **b** IR spectra of the four points studied

WPI and WPIT are amorphous as to the presence of two amorphous halos, centered at 19.2º and 21.0º, respectively. The PBAT diffractogram (Fig. 7a) showed peaks at 16.4º, 17.6º, 20.7º, 23.4º and 25.1º, which were associated with the baseline reflections of the PBAT crystalline phase in (011), (010), (101), (100) and (111), respectively [18]. PBAT/WPIT blends presented the same peaks as PBAT.

The crystallinity degree of the blends reduced with the addition of WPIT. Moreover, the crystallinity degree of the PBAT phase in the blends also decreased slightly in comparison to pristine PBAT, as shown in Fig. 7b. This is additional evidence of the improvement of system miscibility as it can affect the crystallization process [46].

Figure 8 shows the TG (a) and DTG (b) curves for PBAT/WPIT blends. Table 4 presents the onset temperature (Tonset), which is the extrapolated start of each mass loss event and the peak temperature (Tpeak), which corresponds to maximum mass loss variation [47].

Thermal decomposition of WPIT consists of three steps: elimination of remaining water, plasticizer volatilization and breakage of peptide bonds [6, 27]. The TG curve of WPIT (Fig. 8a) shows three stages of degradation between 25 and 600 °C. The first stage of degradation started at room temperature and is associated with removal of water, which usually occurs below 200 °C [48]. The second stage started at 253 °C, which presented one shoulder on the DTG curve at 278 °C and a peak at 313 °C, which coincides with the DTG peak of PEG at 315 °C. One of the protein degradation stages shows a peak at 309 °C for WPI, which is overlapped by the peak of PEG evaporation on the WPIT curve. WPI and WPIT have degradation stages from 280 to 500 °C, which occur due to the degradation of the main constituents of protein [44]. The PBAT sample presents a single degradation stage that started at 383 °C and DTG peak temperature at 408 °C as expected, since, in general, PBAT presents only a single stage of degradation that starts around 350 °C [18]. Both blends showed an evaporation stage of residual water below 200 °C. The 90_10 blend presented the degradation stage from 380 °C relative to PBAT decomposition. The 70_30 blend showed two more stages, a second stage that starts at 255 °C, relative to decomposition of WPIT, and a third peak at 406 °C due to the degradation of the PBAT phase.

TGA additivity curves were obtained for the blends considering the contribution in mass (%) of each component of the blend (Fig. 8c and d). If there are interactions between PBAT and WPIT as chemical reactions, the DTG curves of the blends will not follow the pattern of the additivity curves. A greater loss of moisture was expected for the blends, as shown by the additivity curves, which did not happen as shown in Fig. 8c. Moisture present in the WPIT phase of the blends could be lost during the processing. A normalized curve (Fig. 8d) was obtained to analyze additivity without the mass loss by evaporation of the moisture present in the WPIT phase. Both blends presented improvement in thermal stability in relation to additivity in the PEG evaporation region. As shown by the AFM-IR results, there was a band shift and conformation change of protein phase

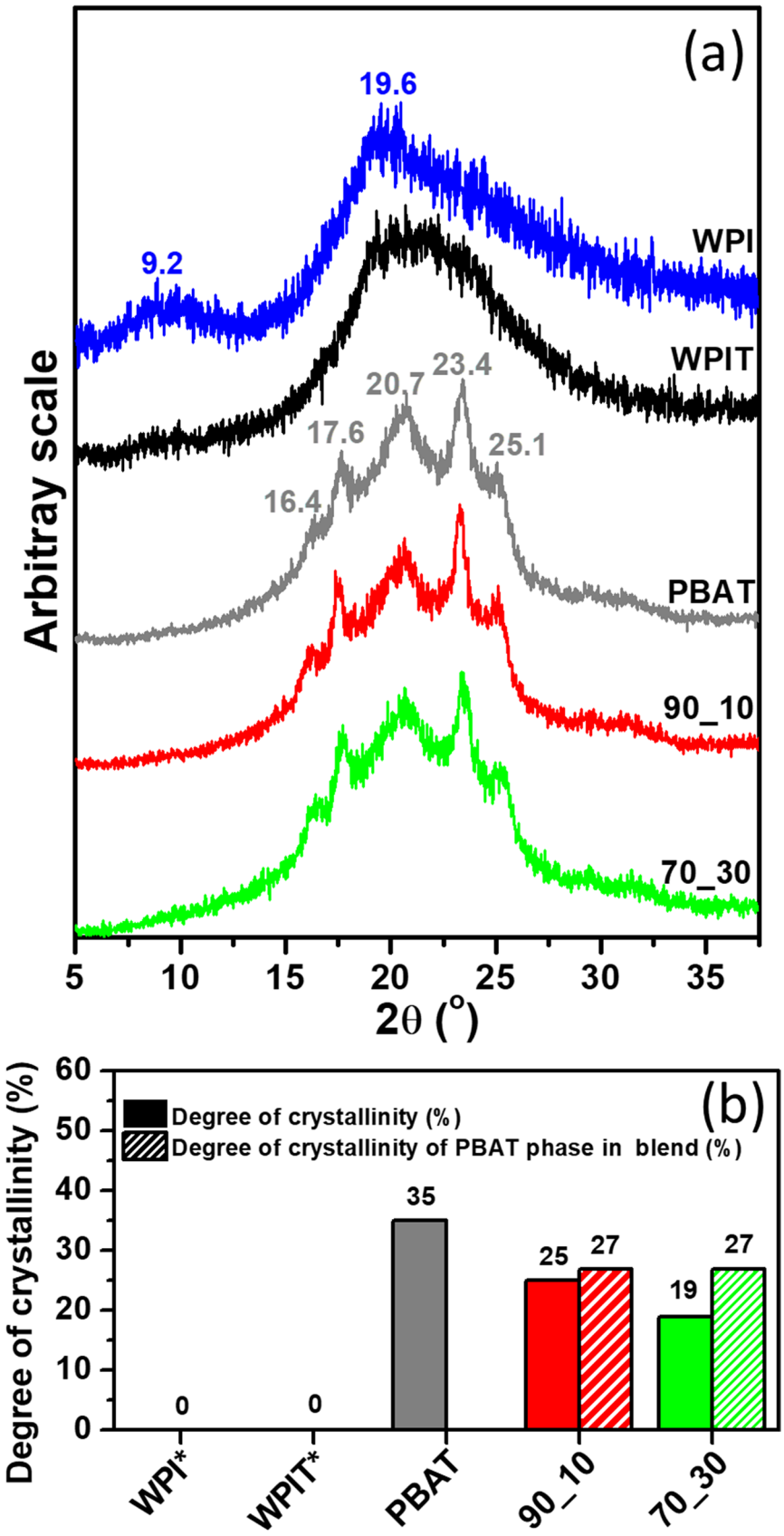

Fig. 7 Results of XRD analyses: **a** XRD diffractograms and **b** degree of crystallinity of PBAT/WPIT blends, PBAT, WPIT and WPI. *WPI and WPIT are amorphous

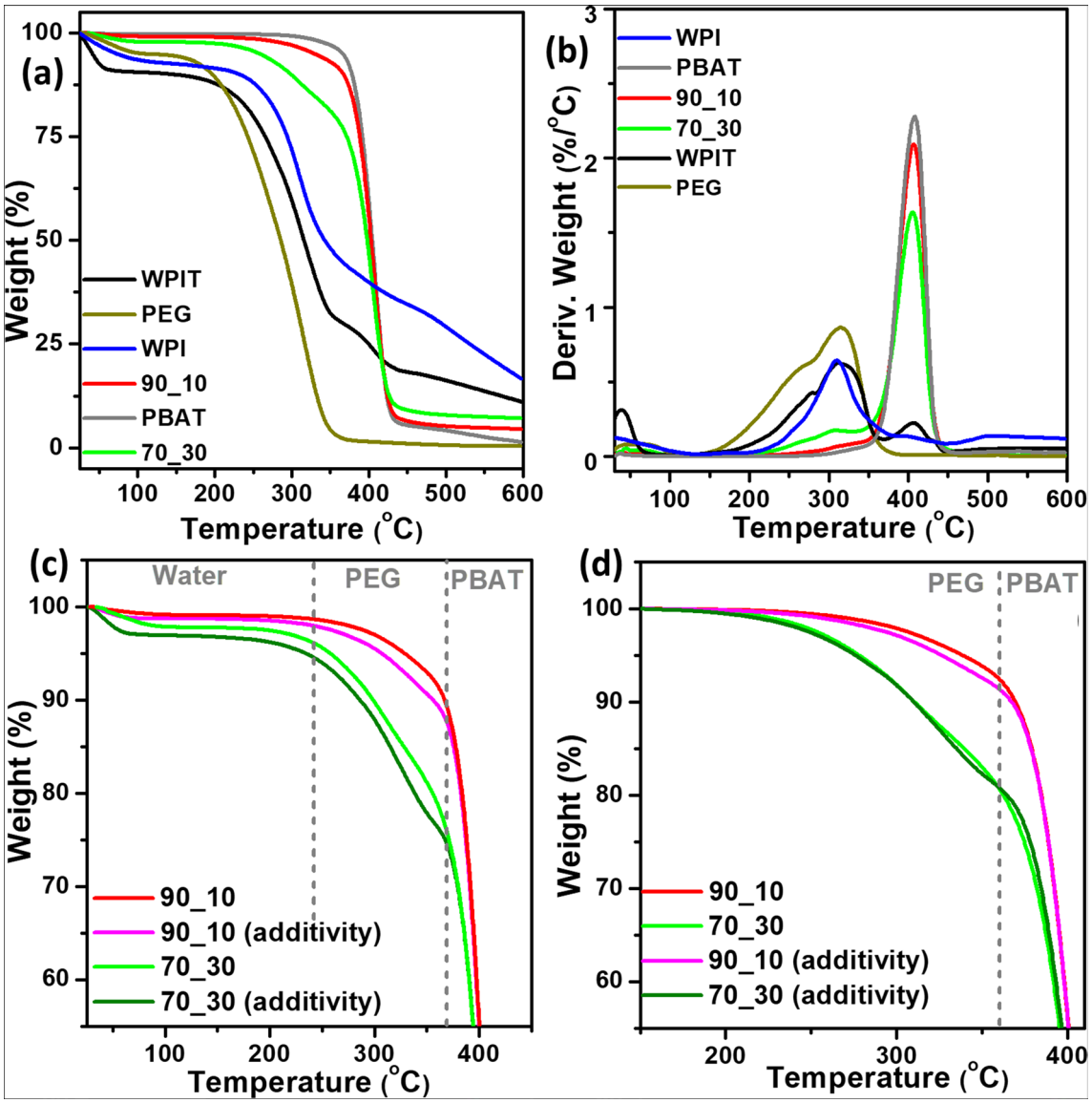

Fig. 8 Results of TGA analyses: **a** TG and **b** DTG curves of PBAT/WPIT blends. Additivity and TG curves of PBAT/WPIT blends **c** plotted as obtained and **d** normalized not considering the water loss

Table 4 Results of PBAT/WPIT blends of TGA (Tonset, Tpeak) and DSC (Tg, Tm PBA, Tm PBT, Tc PEG, Tm PEG and T endothermic peak)

Sample	Tonset* (°C)	Tpeak** (°C)	Tg (°C)	Tm$^{\Delta}$ PBA (°C)	Tm $^{\Delta}$ PBT (°C)	Tc^{o} PEG (°C)	Tm $^{\Delta}$ PEG (°C)	T endothermic peak (°C)
WPI	28/272/-	31/309/392/502	–	–	–	–	–	136
WPIT	31/253/-	39/278;313/407/-	–	–	–	− 34	− 14	123
PBAT	-/-/383	-/-/408	− 34	52	123	–	–	–
90_10	39/-/380	41/319/408	− 35	50	140	–	–	121
70_30	40/255	58/306/406	− 35	47	130	–	− 13	109

Δ *Tm* melting temperature, o *Tc* crystallization temperature

*Tonset (extrapolated beginning of each mass loss event) = Tonset1/Tonset2/Tonset3

**Tpeak (maximum variation of mass loss) = Tpeak1/Tpeak2/Tpeak3

structure in the blends. The formation of other interactions between protein and PEG can reduce chain mobility, which would impair plasticizer evaporation and could increase the thermal stability of the blends in relation to the additivity curves. In the PBAT decomposition region, the 90_10 blend followed the additivity, while the 70_30 blend presented a slight reduction in thermal stability, which could be caused by the existence of PEG chains at the stage of PBAT decomposition due to certain miscibility between a part of PEG and PBAT chains.

DSC heating results for the samples are shown in Fig. 9 and Table 4. Tg of PBAT was found at − 34 °C. The blends present only Tg of the PBAT phase. Tg of the protein phase in the blends and WPIT was not detected by DSC.

In general, miscibility can be detected by obtaining a single intermediate Tg between the Tg of blend components. Although the measurement of Tg is simple, the uncertainties in its measurement must be analyzed. For blends that present content of second component below 10% by mass, the measurement of Tg and its use for detecting blending miscibility are imprecise [42]. In this work, the pristine protein content, without PEG, was below 10% for the 90_10 blend and around 10% for the 70_30 blend. Tg of the protein phase in these blends was difficult to detect by DSC.

Endothermic peak of WPIT occurs at 123 °C, which is due to residual moisture [28] and, in blends, is less pronounced and may be overlapped on the PBAT peaks. WPIT presents an exothermic peak at -34 °C, followed by an endothermic peak at − 14 °C that could be related to PEG, as Tg of PEG was described to occur about − 78 °C and its crystallization and melting appear below − 3 °C [49]. Differences in these transitions could be due to interactions between protein and plasticizer. The 70_30 blend showed a PEG melting stage at − 13 °C. For PBAT and blends there is an endothermic peak at around 50 °C related to the melting of crystalline domains of poly (butylene adipate) (PBA) structure in the PBAT phase. The structure of poly (butylene terephthalate) (PBT) in PBAT and blends is represented by endothermic peaks in the range of 120 to 140 °C due to the melting of its crystalline structures α and β [20, 50].

Elastic modulus, tensile strength at break, and elongation at break of the blends are shown in Table 5. Elastic

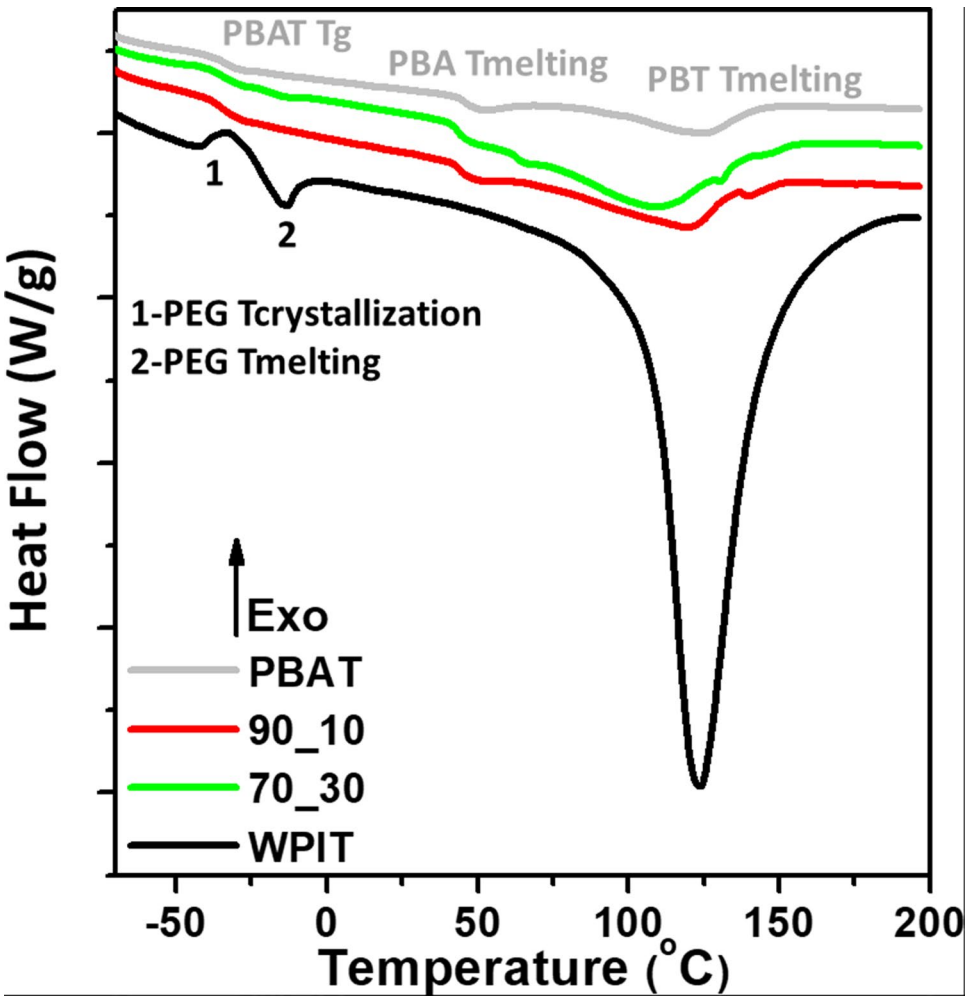

Fig. 9 DSC results of heating step after cooling of PBAT/WPIT blends

Table 5 Tensile test results of PBAT/WPIT blends and PBAT: elastic modulus, tensile strength at break, and elongation at break

Sample	Elastic modulus (MPa)*	Tensile strength at break (MPa)*	Elongation at break (%)*
PBAT	80 ± 3 a	15 ± 1 a	884 ± 101 a
90_10	75 ± 6 b	9 ± 4 b	564 ± 131 b
70_30	94 ± 10 c	7 ± 1 b	276 ± 26 c

*Considering confidence interval (CI) equal to 95%, means values with the same letter do not vary significantly

modulus increased with the addition of WPIT in the PBAT matrix. Moreover, there was a reduction of elongation at break and tensile strength with the addition of WPIT. The joint observations of the morphology of both SEM and AFM-IR and the mechanical properties are consistent for a partially miscible blend. The solubility between them is greater for a low concentration of one of the components than for a higher concentration, reflecting morphology with visual homogeneity and reduction in the elasticity modulus, as for the 90_10 blend. The domains observed for the 70_30 blend (phase rich in WPIT and plasticizer) act as defects causing accentuated decrease in tensile strength and elongation. In addition, it is the phase with a high concentration of plasticizer subject to exudation. Plasticizer is used to facilitate the processing of proteins and to improve the mobility of their molecules, since they are considered rigid materials [6]. During blend cooling after processing, miscibility of the PBAT-WPI-PEG system could decrease, as was visually verified in the blends where PEG undergoes exudation. Plasticizer exudation caused the reduction of plasticizer concentration in the blend, which resulted in the prevalence of protein stiffness, which explains the increase in blend elastic modulus.

The oxygen transmission rate (OTR) and oxygen permeability coefficient ($P'O_2$) of the blends are shown in Table 6. The addition of 30% of WPIT reduced the oxygen permeability coefficient by 20% in relation to pristine PBAT. WPIT has polar side groups, such as amino, carbonyl, carboxyl and hydroxyl radicals, which increase the cohesive energy of polymer molecules, reduce the diffusion coefficient, and enhance the barrier of these materials to gases, such as oxygen [51]. The presence of hydrogen bonds in WPIT greatly contributes to reducing the oxygen permeability of films [52].

Moreover, other authors observed a reduction in PBAT oxygen permeability due to the addition of other compounds such as blends of PBAT/PBS with the proportion of 75/25, which showed a reduction of 29% in oxygen permeability [53]. In another study, PBAT was modified by its copolymerization with 12 mol% of sulfonated units, which showed a reduction in oxygen permeability of about 43% [54]. These works showed that this property is strongly influenced by the PBAT modification system. To analyze the efficiency of our system we considered the work by Schmid et al. [15]. The authors studied a 50/50 blend of EVA and WPIT plasticized with glycerol that decreased the oxygen permeability by 93%. They reported the oxygen permeability of pure WPIT as 52.3 $cm^3m^{-2}d^{-1}$ bar^{-1}. If we assume a similar value for the WPIT prepared in our work, we can apply the rule of mixtures to predict the oxygen permeability of the blends by the mass contribution of each component. The calculated results, shown in Table 6, are: 64.4 mL mm m^{-2} day $^{-1}$ atm for the 90/10 blend, close to the experimental value of 69.7 mL mm m^{-2} day $^{-1}$, and 50.1 mL mm m^{-2} day $^{-1}$ for the 70/30 blend, also in good agreement with the experimental value of 57.1 mL mm m^{-2} day $^{-1}$. This analysis is not accurate, but it helps to reinforce the evidence of partial miscibility between the PBAT and WPIT blends.

The water vapor transmission rate (WVTR) and water vapor permeability coefficient (WVP) of the blends are shown in Table 7. WPIT presents decreased hydrophobicity due to protein unfolding and loss of native conformation after denaturation at 90 °C [55]. The addition of WPIT to the blend increased WVP because it increases blend hydrophilicity, which enhances its water vapor solubility and reduces its barrier to water vapor.

Conclusions

In this work we showed that a protein plasticizer may be used as a blend compatibilizer as well. Polyethylene glycol (PEG) presented chemical affinity with WPI as well as PBAT, as shown by Flory Huggins interaction parameters of 0 and 0.2,

Table 6 Oxygen transmission rate (OTR) and oxygen permeability coefficient ($P'O_2$) of blends at 23 °C and 50% RH

Sample	OTR_1 (mL m^{-2} day^{-1})	OTR_2 (mL m^{-2} day^{-1})	$P'O_{2\_1}$ (mL mm m^{-2} day $^{-1}$ atm)	$P'O_{2\_2}$ (mL mm m^{-2} day $^{-1}$ atm)	$P'O_{2average}$ (mL mm m^{-2} day $^{-1}$ atm)	$P'O_2$ reduction (%)	$P'O_2$ (mL mm m^{-2} day $^{-1}$ atm)*
PBAT	227.8	221.2	71.5	71.4	71.5 ± 0.1	–	–
90_10	190.2	230.6	69.6	69.9	69.7 ± 0.2	3	64.4
70_30	183.0	173.4	56.2	58.1	57.1 ± 1.3	20	50.1

*Values obtained by calculating the mass contribution of each blend component (rule of mixtures)

Table 7 Water vapor transmission rate (WVTR) and water vapor permeability coefficient (WVP) of blends at 38 °C/90% RH

Sample	$WVTR_1$ (g m^{-2} day^{-1})	$WVTR_2$ (g m^{-2} day^{-1})	WVP_1 (g mm m^{-2} day^{-1} $mmHg^{-1}$)	WVP_2 (g mm m^{-2} day^{-1} $mmHg^{-1}$)	$WVP_{average}$ (g mm m^{-2} day^{-1} $mmHg^{-1}$)
PBAT	109.0	103.3	0.8	0.9	0.8 ± 0
90_10	117.1	106.7	1.0	0.8	0.9 ± 0.1
70_30	202.9	197.4	1.4	1.4	1.4 ± 0

respectively. PEG was used as a plasticizer to modify WPI in a thermoplastic material, and it presents some evidence of providing partial miscibility in PBAT/WPIT blends, according to SEM and AFM-IR results. The presence of PBAT and WPIT bands was observed in the dispersed phase and matrix besides adhesion in the phases interface. The viscosity ratio of the PBAT/WPIT system was less than 3.5, which suggests that droplet break-up of WPIT occurred by the drop fibrillation mechanism in the high shear rate region of the torque rheometer. The addition of WPIT improved the oxygen barrier of the blends, with an observed reduction of 20% in the oxygen permeability coefficient for a blend with 30% of WPIT in comparison with PBAT. Although mechanical properties were not improved in a significant way, the addition of WPIT to the blend enhanced elastic modulus and decreased elongation at break and tensile strength.

The elastic component contribution of WPIT prevailed in the molten state, mainly for low shear rates as shown by parallel plate rheometry. This could be caused by strong interactions between the protein chains such as electrostatic interactions that this study did not investigate in a localized manner. Changes in WPIT melting behavior aimed at reducing these interactions could help in improving the compatibilization of PBAT/WPIT systems and, consequently, in mechanical and barrier properties. This subject can be addressed in future works.

Acknowledgements The authors are grateful to the Brazilian Nanotechnology National Laboratory (LNNano/CNPEM) for the use of material characterization (SEM, AFM-IR, tensile tests) and polymer processing facilities, and to the National System of Laboratories for Nanotechnology (SisNANO/MCTI) for its financial support in infrastructure and equipment at the LNNano. Marina Cosate de Andrade thanks CNPq (Process Number 163257/2015-9) for the fellowship. This study was partly financed by Coordenação de Aperfeiçoamento de Pessoal de Nível Superior – Brasil (CAPES) – Finance Code 001. Leo Santos (Rhodia), Vinicius Tanganeli (Rhodia), Aparecida Patreze (CENA/USP), Liz de Moraes (CENA/USP), Suzane Dionísio (CTBE/CNPEM), Carlos Costa (LNNano/CNPEM), Cleyton Biffe (LNNano/CNPEM), and Mathias Strauss (LNNano/CNPEM) are thanked for they support in material analyses and valuable discussions.

Author Contributions M.F.C.A. performed the experiments and wrote the manuscript. H.C.L. prepared the samples for AFM-IR experiments. C.I.G.L.S. performed the oxygen permeability and water vapor permeability analyses. A.R.M. supervised the project. All authors discussed the results and contributed to the final manuscript.

Funding This work was financed by Conselho Nacional de Desenvolvimento Científico e Tecnológico (CNPq) and Coordenação de Aperfeiçoamento de Pessoal de Nível Superior – Brasil (CAPES) – Finance Code 001.

Declarations

Conflict of interest The authors declare that they have no conflict of interest.

References

1. Wilkinson P, Smith KR, Joffe M, Haines A (2007) Lancet 965:978
2. Song F, Tang D-L, Wang X-L, Wang Y-Z (2011) Biomacromol 3369:3380
3. Orliac O, Silvestre F, Rouilly A, Rigal L (2003) Ind Eng Chem Res 1674:1680
4. Schmid M, Dallmann K, Bugnicourt E, Cordoni D, Wild F, Lazzeri A, Klaus N (2012) Int J Polym Sci 1:7
5. Cinelli P, Schmid M, Bugnicourt E, Wildner J, Bazzichi A, Anguillesi I, Lazzeri A (2014) Polym Degrad Stabil 151:157
6. Bier JM, Verbeek CJR, Lay MC (2014) Macromol Mater Eng 524:539
7. Schmid M, Pröls S, Kainz DM, Hammann F, Grupa U (2017) Prog Org Coat 161:172
8. Hernandez-Izquierdo VM, Krochta JM (2009) Packag Technol Sci 255:260
9. Hernandez-Izquierdo VM, Reid DS, Mchugh TH, Berrios JJ, Krochta JM (2008) J Food Sci 169:175
10. Calva-Estrada SJ, Jiménez-Fernández M, Lugo-Cervantes E (2019) Food Eng Rev 78:92
11. Karimi N, Alizadeh A, Almasi H, Hanifian S (2020) Food Sci Technol LEB 1:8
12. Muthuraj R, Misra M, Mohanty AK (2018) J Appl Polym Sci 1:35
13. Azevedo VM, Borges SV, Marconcini JM, Yoshida MI, Neto ARS, Pereira TC, Pereira CFG (2017) Carbohyd Polym 971:980
14. Schmid M, Herbst C, Müller K, Stäbler A, Schlemmer D, Coltelli M-B, Lazzeri A (2016) Polym-Plast Technol 510:517
15. Schmid M, Muller K, Sangerlaub S, Stabler A, Starck V, Ecker F, Noller K (2014) J Appl Polym Sci 1:9
16. Witt U, Einig T, Yamamoto M, Kleeberg I, Deckwer W-D, Müller R-J (2001) Chemosphere 289:299
17. Chivrac F, Kadlecová Z, Pollet E, Avérous L (2006) J Polym Environ 393:401
18. Li G, Shankar S, Rhim J-W, Oh B-Y (2015) Food Sci Biotechnol 1679:1685
19. Mondal D, Bhowmick B, Mollick M, Masud R, Maity D, Saha NR, Rangarajan V, Rana D, Sen R, Chattopadhyay D (2014) J Appl Polym Sci 1:9
20. Herrera R, Franco L, Rodriguez-Galan A, Puiggali J (2002) J Polym Sci A 1(4141):4157

21. Chen F, Zhang J (2010) Polymer 1812:1819
22. Chen F, Zhang J (2009) Polymer 3770:3777
23. Guo G, Zhang C, Du Z, Zou W, Tian H, Xiang A, Li H (2015) Ind Crop Prod 731:736
24. Ajji A (2002). In: Utracki LA (ed) Polymer blends handbook. Kluwer Academic Publishers, Dordrecht, p 295
25. Huang H-X (2011). In: Boudenne A, Ibos L, Candau Y, Thomas S (eds) Handbook of multiphase polymer systems. John Wiley and Sons Ltd, Chichester, p 161
26. Smith MJ, Verbeek CJR (2018) Adv Polym Technol 2354:2366
27. Verbeek CJR, van den Berg LE (2010) Extrusion processing and properties of protein-based thermoplastics. Macromol Mater Eng 295(10):21. https://doi.org/10.1002/mame.200900167
28. Cosate de Andrade MF, Strauss M, Morales AR (2019) J Polym Environ 2131:2143
29. Moustafa H, Guizani C, Dufresne A (2017) J Appl Polym Sci 1:11
30. Krevelen DWV, Nijenhuis KT (2009) Properties of polymers their correlation with chemical structure; their numerical estimation and prediction from additive group contributions, 4th edn. Elsevier, Amsterdam, Oxford
31. Barton AFM (1975) Chem Rev 731:753
32. American Society for Testing and Material (2018) ASTM D1921 − 18. Standard test methods for particle size (Sieve Analysis) of plastic materials.
33. Anasys Instruments, Resonance Enhanced AFM-IR and Tapping AFM-IR. 2016. https://www.anasysinstruments.com/technology/nanoir-technology/. Accessed 01 April 2019
34. American Society for Testing and Material (2017) ASTM E2550-17. Standard test method for thermal stability by thermogravimetry.
35. American Society for Testing and Material (2012) ASTM D882 – 12. Standard test method for tensile properties of thin plastic sheeting.
36. American Society for Testing and Material (2014) ASTM F1927−14. Standard test method for determination of oxygen gas transmission rate, permeability and permeance at controlled relative humidity through barrier materials using a coulometric detector.
37. American Society for Testing and Material (2013) ASTM F1249 – 13. Standard test method for water vapor transmission rate through plastic film and sheeting using a modulated infrared sensor.
38. Coleman MM, Serman CJ, Bhagwagar DE, Painter PC (1990) Polymer 1187:1203
39. Ari GA, Aydin I (2010) J Vinyl Addit Techn 223:228
40. Li G, Favis BD (2010) Macromol Chem Phys 321:333
41. Lin B, Sundararaj U, Mighri F, Huneault MA (2003) Polym Eng Sci 891:904
42. Utracki (2002). In: Utracki LA (ed) Polymer blends handbook. Kluwer Academic Publishers, Dordrecht, p 1
43. Nobrega MM, Olivato JB, Müller CMO, Yamashita F (2012) Polímeros 475:480
44. Ramos ÓL, Reinas I, Silva SI, Fernandes JC, Cerqueira MA, Pereira RN, Vicente AA, Poças MF, Pintado ME, Malcata FX (2013) Food Hydrocolloid 110:122
45. Fabian H, Mantele W (2002) Infrared spectroscopy of proteins. Biochemical applications. John Wiley and Sons, Ltd., Chichester
46. Groeninckx G, Vanneste M, Everaert V (2002) In: Utracki LA (ed) Polymer blends handbook, Kluwer Academic Publishers, Dordrecht, p 203
47. Canevarolo SV (2004) Técnicas de Caracterização de Polímeros, 1st edn. Editora Artliber, São Paulo
48. Barreto PLM, Pires ATN, Soldi V (2003) Polym Degrad Stabil 147:152
49. Molmeret Y, Chabert F, Kissi NE, Iojoiu C, Mercier R, Sanchez J-Y (2011) Polymers 1126:1150
50. Sangroniz A, Gonzalez A, Martin L, Irusta L, Iriarte M, Etxeberria A (2018) Polym Degrad Stabil 25:35
51. Sarantopoulos CIGL, Teixeira FG (2017) Embalagens Plásticas Flexíveis – Principais polímeros e avaliação de propriedades, 2nd edn. ITAL/CETEA, Campinas
52. Schmid M, Prinz TK, Stäbler A, Sängerlaub S (2017) Front Chem 1:15
53. Costa ARM, Crocitti A, Carvalho LH, Carroccio SC, Cerruti P, Santagata G (2020) Polymers-Basel 1:17
54. Huang F, Wu L, Li B-G (2020) Polym Degrad Stabil 1:9
55. Schmid M, Noller K, Wild F, Bugnicourt E (2013) Whey protein coated films. WO 2013/014493 Al.